Synthesis and characterization of new neutral Mn(I) tricarbonyl complexes with 8-hydroxyquinoline and imidazole ligands as CO releasing molecules

Marcel Annereau, Franck Martial, Jérémy Forté, Geoffrey Gontard, Sébastien Blanchard, Héloïse Dossmann, Michèle Salmain, Vincent Corcé

Synthesis and Characterization of new neutral Mn(I) tricarbonyl complexes with 8-hydroxyquinoline and imidazole ligands as CO releasing molecules.

Marcel Annereau, Franck Martial, Jérémy Forté, Geoffrey Gontard, Sébastien Blanchard, Héloïse Dossmann, Michèle Salmain and Vincent Corcé*

Sorbonne Université, CNRS, Institut Parisien de Chimie Moléculaire, IPCM, F-75005 Paris, France.

vincent.corce@sorbonne-universite.fr

Abstract: A series of manganese(I) tricarbonyl complexes formulated as [Mn(8-HQ)$(CO)_3$Imd] (HQ = hydroxyquinoline and Imd = imidazole derivatives) was synthesized and fully characterized. These structures could be easily accessed from a common dimeric edifice formulated as [Mn_2(8-HQ)$_2(CO)_6$]. The structure of this complex has been confirmed by X-ray diffraction studies. Its reaction with a range of imidazole derivatives (Imd) yielded the monomeric complexes [Mn(8-hydroxyquinoline)$(CO)_3$Imd] with various functional groups as an anchoring point for a vector. Photoactivation of all these complexes by blue-light irradiation led to the liberation of 3 mol of CO per mol of complex as determined experimentally. Spectroscopic and computational methods were employed to explore the mechanism of CO release. Finally, a manganese complex including the more elaborate imidazole ligand *N*- and *C*-di-protected histidine was successfully synthesized, opening the way to its direct incorporation in peptides.

Introduction

Carbon monoxide (CO) is a compound with multi-faceted activities. CO has been known for a long time as a dangerous gas to mammals, which earned it the name of “silent killer”.[1] The high toxicity of CO is mainly due to its elevated affinity for the iron present in hemoglobin, leading to the fast formation of carboxyhemoglobin.[2] Intuitively, it appears that all

hemoproteins are sensitive to CO, including vital enzymes involved in oxidative phosphorylation such as cytochrome c oxidase, but CO also possesses multiple non-ferrous targets.[3] On the other hand, the beneficial role of CO in biology is now well established. CO is endogenously generated throughout heme catabolism and acts as a pivotal cell-signalling molecule[4] notably by displaying cell-protective,[5] vasodilatory,[6] and anti-inflammatory effects.[7] To exert a useful therapeutic effect,[8] a proper amount of CO has to be site-specifically delivered and also in a controlled manner to avoid toxic systemic side effects.[9] In its gaseous form, direct use of CO by inhalation would appear to be totally unreasonable and thus, a controlled source of carbon monoxide is required to fully exploit its therapeutic properties. For this purpose, carbon monoxide releasing molecules (CORMs) appeared as an appropriate substitute to CO gas.[10] Several CO carriers and conjugate systems have been elaborated and used for the delivery of CO to mammals[10,11] but also antimicrobial purposes.[12,13] Organic compounds[14] and transition metal carbonyl complexes[9,15,16] represent the two main classes of CORMs developed so far. The growing interest in CORMs stems from the various stimuli that can trigger the CO release, including passive ligand exchange, light irradiation,[17,18] enzyme,[19,20] magnetic heating[21], oxidation[22], or pH.[23] Nevertheless, the use of light remains the most frequently encountered in the literature. Despite recent advances in the field of metal-based CORMs, efforts are still ongoing towards the synthesis of new metal-carbonyl complexes that absorb light in the visible region, a critical point in the prospect of their eventual use for therapeutic purposes. Another critical point to be met by CORMs is their potency of vectorization for the controlled delivery of CO. Indeed, as elegantly stated by Romão and Bernardes,[9] a “drug coordination sphere” featuring an appropriate molecular vector around the metal centre is mandatory for the site-specific delivery of CORMs, but also for improving their pharmacological profile, a prerequisite for the generation of metal-based therapeutics.[24,25] With this in mind, we describe herein the synthesis, structure, and photochemical studies of a new series of photo-

activatable [Mn(8-HQ)$(CO)_3$Imd] with HQ = hydroxyquinoline and Imd = imidazole derivatives. The use of various imidazole-based ancillary ligands allows the synthesis of multiple neutral complexes with a high degree of modularity owing to the presence of allyl, hydroxyl, or amine groups on the imidazole ring that could be further used as anchoring points for the introduction of specific biovectors.

Experimental

Reactions were performed under argon using standard Schlenk techniques. Brown glassware was employed for all reactions. Manganese pentacarbonyl bromide ([$Mn(CO)_5Br$]) was purchased from Strem chemicals. Sodium 8-hydroxyquinolinate ligand was synthesized as described by Marshall.[26] Solvents were freshly distilled before use, according to standard procedures.

Syntheses.

[Mn_2(8-HQ)$_2(CO)_6$] (**1**). Sodium 8-hydroxyquinolinolate (1 equiv., 8.05 mmol, 1.42 g) was solubilized in THF (25 mL) at room temperature and manganese pentacarbonyl bromide ([$Mn(CO)_5Br$]) (1 equiv., 8.05 mmol, 2.336 mg) was added in one portion. The solution was stirred under argon for 4 h at room temperature with exclusion of light. Sodium bromide was filtered off and rinsed with THF (2 mL). The solvent was removed by rotatory evaporation with the heating bath at 25 °C to afford a yellow solid. The product was purified by chromatography on SiO_2 (DCM/MeOH 99:1) yielding the dimer **1** as a yellow powder (1.39 g, 57%). Slow diffusion of pentane into a dichloromethane solution of **1** afforded yellow blade-like crystals suitable for X-ray diffraction analysis. RP-HPLC analysis: Retention time: 5.7 min; purity: 92.4 %. ^{1}H NMR (400 MHz, Methylene Chloride-d_2), δ 7.94 (dd, *J* = 4.9, 1.4 Hz, 2H), 7.68 (dd, *J* = 8.4, 1.4 Hz, 2H), 7.48 (t, *J* = 7.9 Hz, 2H), 7.39 (dd, *J* = 7.7, 1.2 Hz, 2H), 6.93 (dd, *J* = 8.0, 1.2 Hz, 2H), 6.79 (dd, *J* = 8.3, 4.9 Hz, 2H) ^{13}C NMR (75 MHz, Methylene Chloride-d_2) δ 168.1,

151.4, 144.5, 137.0, 129.5, 128.8, 122.1, 117.6, 116.3. IR (ν, cm^{-1}): 2031, 2016, 1926, 1893, 1759. HRMS (ESI), *m/z* calcd. for $C_{24}H_{12}Mn_2N_2O_8$ [M+H^+]: 566.9427. Found: 566.9417.

[Mn(8-HQ)(CO)$_3$Me-Imd] (2). A mixture of [Mn_2(8-HQ)$_2$(CO)$_6$] (1 equiv., 0.3 mmol, 181 mg) and 1-methylimidazole (2 equiv., 0.6 mmol, 72 µL) in THF (3 mL) was stirred for 2 h. The solvent was removed under vacuum, and the residue was washed thoroughly with pentane. The product was purified by chromatography on SiO_2 (cyclohexane/ethyl acetate 4:6) to yield the complex **2** as a yellow powder (181 mg, 77%). Slow diffusion of pentane into a dichloromethane solution of **2** afforded yellow blade-like crystals suitable for X-ray analysis. RP-HPLC analysis: Retention time: 5.75 min; purity: 99.9 %. λ_{max} (nm) (ε ($M^{-1}.cm^{-1}$)) in CH_3CN: 346 (4065), 433 (2692). ^{1}H NMR (300 MHz, Chloroform-*d*) δ 8.93 (d, *J* = 4.5 Hz, 1H), 8.06 (d, *J* = 8.3 Hz, 1H), 7.37 (m, 2H), 7.32 – 7.27 (m, 1H), 7.05 (m, 1H), 6.94 (s, 1H), 6.83 (d, *J* = 7.8 Hz, 1H), 6.65 (s, 1H), 3.49 (s, 3H) ppm. ^{13}C NMR (75 MHz, Chloroform-*d*) δ 147.6, 138.7, 137.0, 130.3, 130.25, 130.1, 121.5, 121.0, 109.4, 34.4 ppm. IR (ν, cm^{-1}): 2026, 1925, 1905. HRMS (ESI^+), *m/z* calcd. for $C_{16}H_{13}MnN_3O_4$ [M+H^+]: 366.02810. Found: 366.02813.

[Mn(8-HQ)(CO)$_3$H-Imd] (3). A mixture of [Mn_2(8-HQ)$_2$(CO)$_6$] (1 equiv., 0.18 mmol, 104.6 mg) and imidazole (2.1 equiv., 0.38 mmol, 226 mg) in THF (6 mL) was stirred for 2 h. The solvent was removed under vacuum, and the residue was washed thoroughly with pentane to afford complex **3** as a yellow powder (83 mg, 67%). Slow diffusion of pentane into a dichloromethane solution of **3** afforded yellow blade-like crystals suitable for X-ray analysis. RP-HPLC: Retention time: 5.76 min; purity: 99.0 %**.** λ_{max} (nm) (ε ($M^{-1}.cm^{-1}$)) in CH_3CN: 348 (6800), 435 (4600). ^{1}H NMR (400 MHz, DMSO-*d*6) δ 12.51 (s, 1H, NH), 9.00 (d, *J* = 4.7 Hz, 1H), 8.24 (d, *J* = 8.3 Hz, 1H), 7.71 (s, 1H), 7.47 (dd, *J* = 8.4, 4.7 Hz, 1H), 7.28 (t, *J* = 7.8 Hz, 1H), 7.05 (s, 1H), 6.96 – 6.52 (m, 3H) ppm. ^{13}C NMR (100 MHz, DMSO-d_6) δ 169.3, 148.2, 143.5, 137.1, 137.0, 129.8, 127.8, 122.3, 117.7, 113.5, 108.6 ppm. IR (ν, cm^{-1}): 2026, 1925, 1905. HRMS (ESI+), *m/z* calcd. for $C_{15}H_{11}MnN_3O_4$ [M+H^+]: 352.0125. Found: 352.0126.

[Mn(8-HQ)(CO)$_3$HO-Et-Imd] (4). A mixture of [Mn_2(8-HQ)$_2$(CO)$_6$] (1 equiv., 0.32 mmol, 181 mg) and 1-(2-hydroxyethyl)imidazole (2 equiv., 0.64 mmol, 72 mg) in THF (3 mL) was stirred for 2 h. The solvent was removed under vacuum, and the residue was washed thoroughly with pentane to yield complex **4** as a yellow powder (196 mg, 77%). Slow diffusion of pentane into a dichloromethane solution of **4** afforded yellow blade-like crystals suitable for X-ray analysis. RP-HPLC: Retention time: 5.73 min; purity: 99.9%. λ_{max} (nm) (ε ($M^{-1}.cm^{-1}$)) in CH_3CN: 347 (5492), 433 (3652). ^{1}H NMR (400 MHz, DMSO-*d*$_6$) δ 8.99 (d, *J* = 4.6 Hz, 1H), 8.25 (d, *J* = 8.3 Hz, 1H), 7.80 (s, 1H), 7.49 (dd, *J* = 8.4, 4.7 Hz, 1H), 7.29 (t, *J* = 7.9 Hz, 1H), 7.10 (s, 1H), 6.81 (t, *J* = 7.5 Hz, 2H), 6.74 (s, 1H), 4.90 (t, *J* = 5.0 Hz, 1H), 3.90 (t, *J* = 5.2 Hz, 2H), 3.51 (q, *J* = 5.1 Hz, 2H) ppm.^{13}C NMR (100 MHz, DMSO-*d*$_6$) δ 169.4, 148.2, 143.6, 139.0, 137.1, 129.8, 127.8, 122.3, 121.1, 113.5, 108.6, 60.0, 49.7 ppm. IR (ν, cm^{-1}): 2019, 1919, 1891. HRMS (ESI^+), *m/z* calcd. for $C_{17}H_{15}MnN_3O_5$ [$M+H^+$]: 418.0208. Found: 418.0208.

[Mn(8-HQ)(CO)$_3$BocNH-Pr-Imd] (5). A mixture of [Mn_2(8-HQ)$_2$(CO)$_6$] (1 equiv., 0.35 mmol, 200 mg) and 1*H*-imidazol-1-yl)propyl)carbamate (2 equiv., 0.7 mmol, 158 mg) in THF (3 mL) was stirred for 2 h. The solvent was removed under vacuum, and the residue was washed thoroughly with pentane. The product was purified by chromatography on SiO_2 gel (DCM/MeOH 99:1) to yield complex **5** as a yellow powder (211 mg, 59%). RP-HPLC: Retention time: 5.77 min; purity: 99.9 %. λ_{max} (nm) (ε ($M^{-1}.cm^{-1}$)) in CH_3CN: 347 (5403), 433 (3644).^{1}H NMR (300 MHz, Chloroform-*d*) δ 8.97 (dd, *J* = 4.8, 1.4 Hz, 1H), 8.07 (dd, *J* = 8.3, 1.4 Hz, 1H), 7.49 (s, 1H), 7.38 (t, *J* = 7.9 Hz, 1H), 7.33 – 7.29 (m, 1H), 7.05 (d, *J* = 7.9 Hz, 1H), 6.95 (s, 1H), 6.84 (d, *J* = 7.9 Hz, 1H), 6.72 (s, 1H), 4.48 (s, 1H), 3.80 (t, *J* = 6.9 Hz, 2H), 3.00 – 2.58 (m, 2H), 1.78 (m, 2H), 1.45 (s, 9H) ppm. ^{13}C NMR (75 MHz, Chloroform-*d*) δ 169.45, 147.7, 144.4, 138.3, 137.0, 130.3, 130.3, 130.2, 121.6, 119.7, 114.55, 109.5, 77.4, 45.3, 31.1, 28.5 ppm. IR (ν, cm^{-1}): 2019, 1909, 1895. HRMS (ESI^+), *m/z* calcd. for $C_{23}H_{26}MnN_4O_6$ [$M+H^+$]: 509.1227. Found: 509.1225.

[Mn(8-HQ)(CO)$_3$Allyl-Imd] (6). A mixture of [Mn_2(8-HQ)$_2$(CO)$_6$] (1 equiv., 0.35 mmol, 200 mg) and allyl imidazole (2 equiv., 0.7 mmol, 75 µL) in THF (3 mL) was stirred for 3.5 h. The solvent was removed under vacuum, and the residue was washed thoroughly with pentane. The product was purified by chromatography on SiO_2 (DCM/MeOH 98:2) to yield complex **6** as a yellow-orange powder (208 mg, 76%). Slow diffusion of pentane into a dichloromethane solution of **6** afforded yellow blade-like crystals suitable for X-ray analysis. RP-HPLC: Retention time: 5.83 min; purity: 98.8 %. λ_{max} (nm) (ε ($M^{-1}.cm^{-1}$)) in CH_3CN: 347 (5937), 433 (3993). ^{1}H NMR (300 MHz, Chloroform-*d*) δ 8.94 (dd, *J* = 4.8, 1.4 Hz, 1H), 8.06 (dd, *J* = 8.3, 1.4 Hz, 1H), 7.44 (s, 1H), 7.37 (t, *J* = 7.9 Hz, 1H), 7.31 – 7.27 (m, 1H), 7.03 (dd, *J* = 7.9, 1.1 Hz, 1H), 6.94 (s, 1H), 6.82 (dd, *J* = 8.0, 1.0 Hz, 1H), 6.66 (s, 1H), 5.86 – 5.65 (m, 1H), 5.19 (d, *J* = 10.3 Hz, 1H), 4.96 (d, *J* = 17.1 Hz, 1H), 4.33 (d, *J* = 5.9 Hz, 2H) ppm. ^{13}C NMR (75 MHz, Chloroform-*d*) δ 169.55, 147.6, 144.5, 138.2, 137.0, 131.4, 130.35, 130.3, 130.1, 121.5, 119.9, 119.8, 114.7, 109.4, 50.4 ppm. IR (ν, cm^{-1}): 2020, 1920, 1897. HRMS (ESI^+), *m/z* calcd. for $C_{18}H_{15}MnN_3O_4$ [$M+H^+$]: 392.0438. Found: 392.0438.

[Mn(8-HQ)(CO)$_3$NAc-His-OMe] (7). A mixture of [Mn_2(8-HQ)$_2$(CO)$_6$] (1 equiv., 0.34 mmol, 192 mg) and di-protected histidine (2 equiv., 0.68 mmol, 144 mg) in THF (5 mL) was stirred for 2 h under reflux. The solvent was removed under vacuum, and the residue was washed thoroughly with pentane. The product was purified by chromatography on SiO_2 (DCM/MeOH 95:5) to yield complex **7** as a yellow powder (106 mg, 32%). Slow diffusion of pentane into a dichloromethane solution of **7** afforded yellow blade-like crystals suitable for X-ray analysis. RP-HPLC: Retention time: 5.79 min; purity: 99.9 %. λ_{max} (nm) (ε ($M^{-1}.cm^{-1}$)) in CH_3CN: 347 (6062), 433 (4094). ^{1}H NMR (400 MHz, Methylene Chloride-d_2) δ 11.87 (s, 1H), 8.95 (d, *J* = 4.7 Hz, 1H), 8.21 – 7.91 (m, 1H), 7.51 – 7.11 (m, 3H), 6.84 (m, 2H), 6.64 (m, 2H), 4.61 (s, 1H), 3.49 (m, 3H), 3.15 – 2.70 (m, 2H), 1.81 (m, 3H) ppm. ^{13}C NMR (101 MHz, Methylene Chloride-d_2) δ 172.0, 169.1, 148.6, 144.6, 137.6, 130.8, 130.5, 127.5, 127.4, 122.3, 114.6, 110.5, 53.0, 52.9,

52.6, 28.7, 23.2 ppm. IR (ν, cm^{-1}): 2023, 1921, 1897. HRMS (ESI^+), *m/z* calcd. for $C_{21}H_{20}MnN_4O$ $[M+H^+]$: 495.0707. Found:495.0705.

X-ray Crystallography.

A suitable crystal was chosen, mounted and placed in a cold nitrogen gas stream. Intensity data was measured with Bruker Kappa APEX II apparatuses equipped with fine-focus sealed tube Mo-Kα radiation (**1**, **2**, **3**) or micro-source Cu-Kα radiation (**4**, **6**, **7**). Bruker APEX2/3 software was used for unit-cell parameters determination, data collection strategy, integration and absorption correction. Olex2 (**1**, **2**, **3**, **4**, **6**) or WinGX (**7**) were used for solving, with SHELXT, and refining, with SHELXL, the crystal structures. Structures and data can be retrieved from the Cambridge Crystallographic Data Centre at www.ccdc.cam.ac.uk. The deposition numbers are 2160591 (**1**), 2160593(**2**), 2160592 (**3**), 2160594 (**4**), 2170555 (**6**) and 2160595 (**7**).

Computational methods.

the GAUSSIAN 16 software was used for Density-functional theory (DFT) calculations.[27] The level of theory PBE0/Def2-TZVP was applied for geometry optimizations, frequency and single-point energy calculations.[28–30] The Polarizable Continuum Model (PCM) model was used to mimic the MeCN solvent effect.[31] The same method was applied for Time-dependent (TD)-DFT calculations. Transitions associated to specific excited states are qualitatively described using natural transition orbitals (NTOs).[32] Computed structures shown in this work are depicted using the Chemcraft software.[33]

Spectroscopic measurements.

Cary 50 (Varian) spectrophotometer was used to record the absorption spectra, under controlled temperature. Complexes were solubilized in DMSO at a final concentration of 10 mM and stored in the dark at - 20 °C. Bruker Avance III HD-400 or Bruker Avance III 300 spectrometers were employed for the acquisition of NMR spectra. ^1H NMR peaks were calibrated using the residual solvent peak as reference. Coupling constants (*J*) are given in Hz

and chemical shifts (δ) in ppm. Infrared (IR) spectra were recorded on Tensor 27 FT-IR spectrometer (Bruker) at 4 cm^{-1} resolution equipped with an ATR accessory. *In situ* IR was performed with a React-IR 15 apparatus (Mettler Toledo) equipped with an MCT detector using HappGenzel apodization to collect IR reaction spectra. The instrument was fitted with a DiComp (Diamond) probe connected via 6 mm x 1.5 m silver halide fibre. All data was collected at 8 cm^{-1} resolution from 4000 to 650 cm^{-1}. Scan intervals ranged from 0.5 to 1 min. An air background was collected prior to the experiments and Mettler Toledo iCIR version 4.3 was used for instrument control and data analysis. Characterisation of the samples was done by recording high-resolution mass spectra (HRMS) with a LTQ Orbitrap XL (Thermo Fisher Scientific) instrument equipped with an electrospray ion source in the positive mode. Analytical reverse phase HPLC was performed on an instrument comprising PU-2080 and PU-2087 pumps and UV-2075 detector (Jasco) using a Nucleodur C18ec column, 5 µm, 150 x 4.6 mm, 100Å (Macherey-Nagel) with H_2O / MeOH 3:7 as mobile phase at 0.8 mL/min with detection set at 254 nm. Injection volume: 20 µL of a 100 µM solution in MeOH. X-band EPR spectra were recorded in non-saturating conditions on a Bruker ELEXSYS 500 spectrometer equipped with an Oxford instrument continuous-flow liquid-helium cryostat and a temperature control system. Typical conditions were: 20K, 1G amplitude modulation, 9.40 GHz, microwave power: 1.26 mW.

Quantification of CO release.

Standard Myoglobin assay was used for the quantification of the liberation of CO release.[34] The amount of released CO was determined by calculation of the carboxymyoglobin (MbCO) concentration with the following equation:[35]

$$[MbCO]_t = \left(\frac{Abs_t}{l} - \frac{Abs_{t0}}{l}\right) * \frac{1}{\left(\varepsilon_{540nm(MbCO)} - \frac{Abs_{t0}}{[Mb]_0 * l}\right)}$$

With Abs_t = absorption at a given time *t*, Abs_{t0} = absorption at *t* = 0, l = pathlength of the cuvette, $\varepsilon_{540nm(MbCO)}$ = molar extinction coefficient of myoglobin at 540 nm (15 400 $L.M^{-1}.cm^{-1}$), $[Mb]_0$ = initial concentration of myoglobin.

Results and discussion

Syntheses. To design new photo-activatable manganese-based CORMs, we turned our attention to imidazole and 8-hydroxyquinoline (8-HQ) as interesting ligand candidate. The 8-HQ ligand, also called oxine, is indeed a well-known structure in analytical chemistry that exhibits excellent coordinating abilities and can therefore afford various complexes with a panel of metal ions.[36] In addition, the resulting complexes often present a metal-to-ligand charge transfer (MLCT) leading to absorption into the visible region of the electromagnetic spectrum. Finally, oxine can also be easily functionalized to modulate its photophysical properties. In the same vein, Mansour disclosed the synthesis of Mn-based photoCORMs with 8-aminoquinoline ligand, showing the high interest of these particular 8-substituted quinoline structures.[37] Seminal works of Parker and Wojcicki[38,39] described the synthesis of Mn(8-HQ)$(CO)_4$ from sodium 8-hydroxyquinolinate and manganese pentacarbonyl bromide. During their investigations, they demonstrated that one carbonyl ligand could be replaced by phosphines or amines, leading to the corresponding manganese tricarbonyl complexes. As a starting point, we therefore planned to reproduce this work and replace one carbonyl group with an imidazole ligand. As depicted in scheme 1, the first step consisted in the formation of sodium 8-hydroxyquinolinate by treatment of commercial 8-hydroxyquinoline with sodium hydroxide in acetone. The next step involved direct reaction of sodium hydroxyquinolinate with $Mn(CO)_5Br$ to yield Mn(8-HQ)$(CO)_4$. After several attempts, in our hands, the desired manganese tetracarbonyl complex could not be obtained, but we rather isolated a dimeric structure formulated as $[Mn_2(8\text{-}HQ)_2(CO)_6]$ (**1**). This dimer undergoes a fast solvolysis in coordinating solvents such as acetonitrile, tetrahydrofuran or water but remains relatively

stable in dichloromethane. Surprisingly, it could also be purified, with exclusion of light, by chromatography on SiO_2.

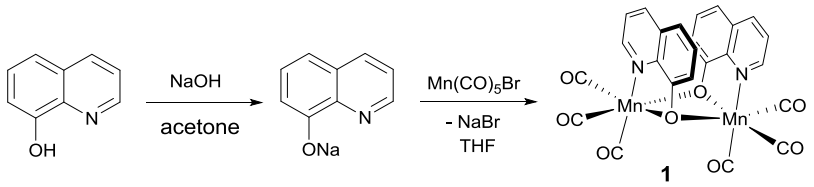

Scheme 1. Synthesis of the dimeric $Mn_2(8\text{-HQ})_2(CO)_6$ complex **1**.

The dimeric structure of **1** was secured through the obtention of single crystals suitable for X-ray diffraction (Figure 1). This structure is in line with the work reported by Ertem, Grills and Rochford where a similar manganese dimeric structure with the parent ligand 5,7-dimethyl-8-oxyquinolate was proposed.[40] It is noteworthy that comparable dimeric structures of rhenium complexes with hydroxyquinoline ligands were also reported.[41,42] In these works, the manganese or rhenium dimeric structures could be converted into monometallic complexes through the addition of an external co-ligand. Based on these observations, we applied a series of imidazole ligands with different functional groups. Treatment of **1** with N-substituted imidazole ligands in tetrahydrofuran at room temperature afforded new mononuclear manganese complexes formulated as $[Mn(8\text{-HQ})(CO)_3Imd]$ in good yield (Scheme 2). The reaction proceeded smoothly and the corresponding complexes **2**, **4**, **5** and **6** respectively comprising *N*-substituted imidazole bearing methyl, hydroxyethyl, Boc-protected aminopropyl or allyl groups were isolated after silica gel chromatography. Introduction of hydroxyl or amine functional groups in **4** and **5** respectively could allow a functionalization of the complexes through an ester or amide linkages. In addition, introduction of an allyl moiety in complex **6** could be used as a precursor for cross-coupling metathesis. Complex **3** derived from unsubstituted imidazole could also be isolated, suggesting that imidazole-containing compounds such as histidine could be envisioned as ligands. In this vein, reaction of dimer **1** with *N*- and *C*- protected histidine afforded the histidine-based manganese tricarbonyl

complex **7**. In a similar approach, a more complex protocol was reported by Schatzschneider and Simpson by combining azole derivatives with $Mn(CO)_3(bpy)Br$ and silver triflate, affording the cationic complexes $[Mn(CO)_3(bpy)(azole)]OTf$ after bromide abstraction.[43]

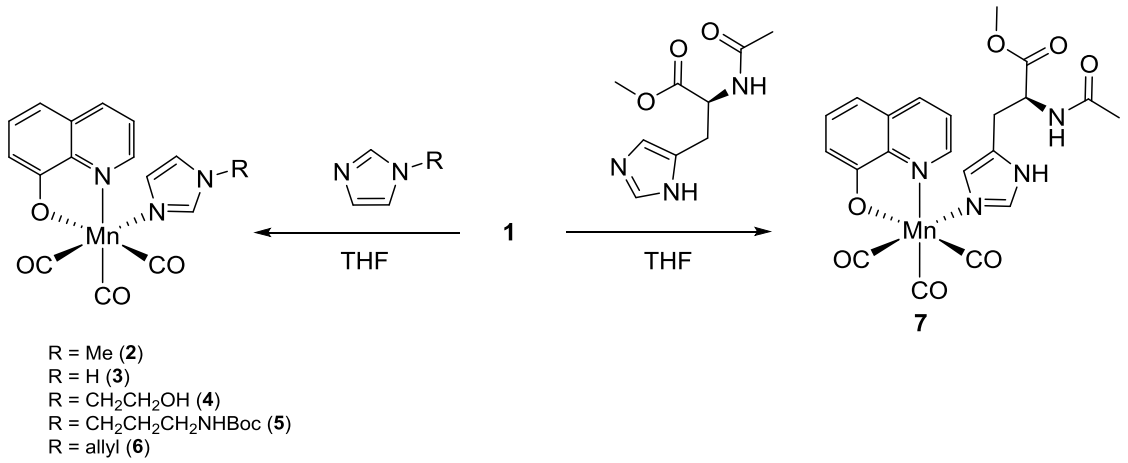

Scheme 2. Synthetic pathway for imidazole-based manganese tricarbonyl complexes **2-6** and histidine-based manganese tricarbonyl complex **7**.

Crystal structures analysis. Yellow single crystals of **1**, **2**, **3**, **4**, **6** and **7** were grown after slow vapor diffusion of pentane into a dichloromethane solution of each compound at room temperature. Their molecular structure was determined using X-ray diffraction (XRD). Because of their photosensitivity, crystallization, storage and analysis, were conducted with exclusion of light. Under these conditions, dimeric complex **1** crystallized in $P2_12_12_1$ space group (orthorhombic system). Unit cell is made up of four molecules and the asymmetric unit comprises one complete molecule. Crystal data and structure refinement parameters are available in Table S1. Structure of **1** (Figure 1) shows that each monomeric part is crystallographically-independent and the aromatic rings are face-to-face. The Mn-Mn intermetallic distance (3.1667(4) Å) is located in the median class interval (Figure S1) observed in the CSD database with the Data Analysis module of *Mercury* software.[44] The coordination sphere around each manganese atom shows an octahedral geometry, where three CO ligands are connected in facial (*fac*) way. The nitrogen atom of (8-HQ) ligand occupies the other axial position and its oxygen atom completes the coordination polyhedron in the equatorial plane by bridging both monomers (Mn-O-Mn angles are 99.95(6)° and

100.58(6)°).Thus, two μ2-O symmetric bridges are formed and Mn1, O1, Mn2, O5 almost lie in a same slightly distorted plane (O1-Mn1-O5-Mn2 torsion angle = 10.14(6)°). Finally, an intramolecular π-π stacking interaction can be observed between both (8-HQ) ligands (bond length between each *N*-heterocycle centroid = 3.6855(13) Å).[45] Bond lengths and angles around Mn atoms for **1** can be found in Table S2. Complexes **2**, **6** and **7** crystallized in P-1 (triclinic) space group whereas complexes **3** and **4** crystallized in $P2_1/c$ (monoclinic) and Pbca (orthorhombic) space groups respectively. More data concerning the structure refinement and crystals are available in Table S1. These crystal structures are displayed in Fig. 2-6. They all exhibit a similar slightly distorted octahedral geometry around the manganese with facial coordination of the three CO ligands, as frequently observed for $MnL_A(\eta^2)(CO)_3L_B(\eta^1)$ complexes. The η^2-coordination of the (8-HQ) ligand in these complexes is similar to the one observed for **1** (N-Mn-O bond angles close to 80°). The η^1-imidazole group completes the coordination sphere in the equatorial plane by its nitrogen atom in position 3 of the heterocycle. Concerning **3**, **4** and **7**, intermolecular H-bonds are present (one for **3** and **4**, two for **7**).

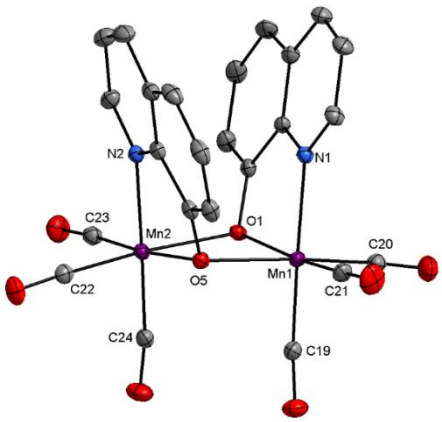

Figure 1. Crystal structure representation of **1** (CCDC 2160591). Ellipsoids are drawn with 30% probability. Hydrogen atoms are omitted for the sake of clarity.

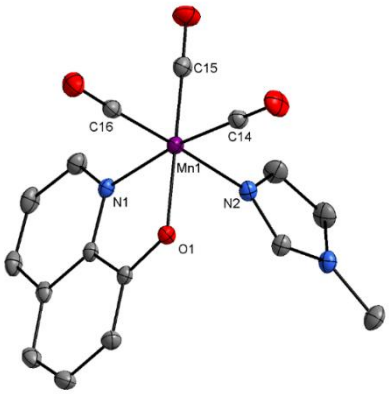

Figure 2. Crystal structure representation of **2** (CCDC 2160593). Ellipsoids are drawn with 30% probability. Hydrogen atoms are omitted for the sake of clarity. Bond lengths (Å) and angles (°) in the coordination sphere at 200 K : Mn1-O1 2.0105(9), Mn1-N1 2.0513(11), Mn1-C14 1.8146(14), Mn1-C15 1.7996(14), Mn1-C16 1.8022(14), Mn1-N2 2.0760(11), O1-Mn1-N1 81.10(4), O1-Mn1-C14 90.93(5), O1-Mn1-C15 177.46(5), O1-Mn1-C16 92.19(5), O1-Mn1-N2 85.24(4), N1-Mn1-C14 171.79(5), N1-Mn1-C15 96.94(5), N1-Mn1-C16 93.32(5), N1-Mn1-N2 86.74(4), C14-Mn1-C15 90.96(6), C14-Mn1-C16 88.96(6), C14-Mn1-N2 90.62(5), C15-Mn1-C16 89.54(6), C15-Mn1-N2 93.04(5), C16-Mn1-N2 177.39(5).

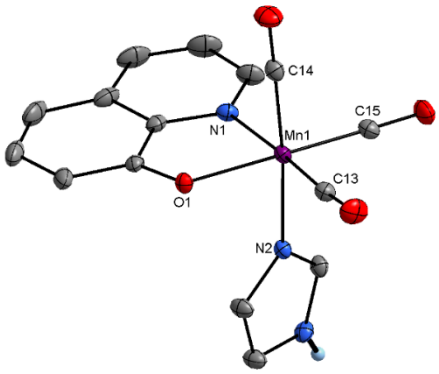

Figure 3. Crystal structure representation of **3** (CCDC 2160592). Ellipsoids are drawn with 30% probability. Most of hydrogen atoms are omitted for the sake of clarity. Only the hydrogen atom involved in hydrogen bond is shown. Bond lengths (Å) and angles (°) in the coordination sphere at 200 K : Mn1-O1 2.0188(10), Mn1-N1 2.0386(13), Mn1-C13 1.8105(16), Mn1-C14 1.8018(17), Mn1-C15 1.7928(16), Mn1-N2 2.0731(13), O1-Mn1-N1 80.79(5), O1-Mn1-C13 94.62(6), O1-Mn1-C14 91.45(6), O1-Mn1-C15 176.95(6), O1-Mn1-N2 84.71(5), N1-Mn1-C13 175.12(6), N1-Mn1-C14 88.66(6), N1-Mn1-C15 96.56(7), N1-Mn1-N2 87.03(5), C13-Mn1-C14 89.81(7), C13-Mn1-C15 88.07(7), C13-Mn1-N2 94.23(6), C14-Mn1-C15 89.98(7), C14-Mn1-N2 174.63(6), C15-Mn1-N2 93.68(6).

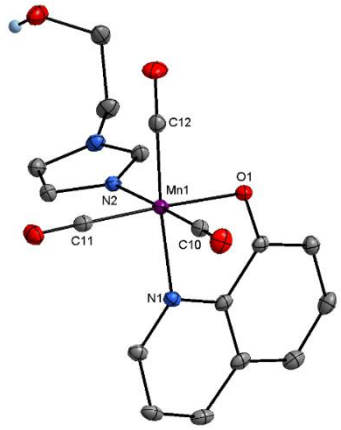

Figure 4. Crystal structure representation of **4** (CCDC 2160594). Ellipsoids are drawn with 30% probability. Most of hydrogen atoms are omitted for the sake of clarity. Only the hydrogen atom involved in hydrogen bond is shown. Bond lengths (Å) and angles (°) in the coordination sphere at 150 K : Mn1-O1 2.0275(16), Mn1-N1 2.046(2), Mn1-C10 1.813(3), Mn1-C11 1.801(3), Mn1-C12 1.796(3), Mn1-N2 2.084(2), O1-Mn1-N1 80.95(7), O1-Mn1-C10 96.07(9), O1-Mn1-C11 173.84(9), O1-Mn1-C12 93.04(9), O1-Mn1-N2 85.35(7), N1-Mn1-C10 92.21(9), N1-Mn1-C11 94.97(10), N1-Mn1-C12 173.91(10), N1-Mn1-N2 87.35(8), C10-Mn1-C11 88.66(11), C10-Mn1-C12 89.40(11), C10-Mn1-N2 178.44(10), C11-Mn1-C12 90.94(11), C11-Mn1-N2 89.88(10), C12-Mn1-N2 91.19(10).

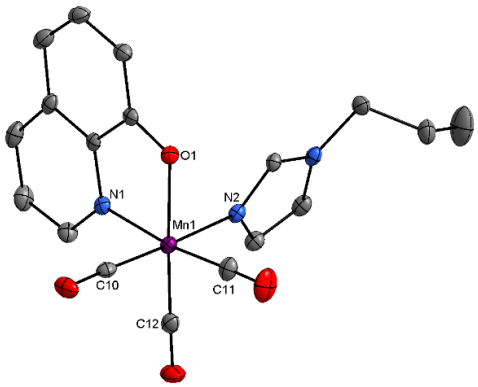

Figure 5. Crystal structure representation of **6** (CCDC 2170555). Ellipsoids are drawn with 30% probability. Hydrogen atoms are omitted for the sake of clarity. Bond lengths (Å) and angles (°) in the coordination sphere at 200 K : Mn1-O1 2.0073(15), Mn1-N1 2.0471(19), Mn1-C10 1.794(2), Mn1-C11 1.806(3), Mn1-C12 1.793(3), Mn1-N2 2.0734(18), O1-Mn1-N1 81.40(7), O1-Mn1-C10 93.69(8), O1-Mn1-C12 175.98(8), O1-Mn1-C11 90.99(11), O1-Mn1-N2 85.32(7), N1-Mn1-C10 90.87(9), N1-Mn1-C12 97.56(10), N1-Mn1-C11 172.37(10), N1-Mn1-N2 86.44(7), C10-Mn1-C12 90.21(10), C10-Mn1-C11 90.1(1), C10-Mn1-N2 177.25(9), C11-Mn1-C12 90.01(11), C12-Mn1-N2 90.74(9), C11-Mn1-N2 92.49(9).

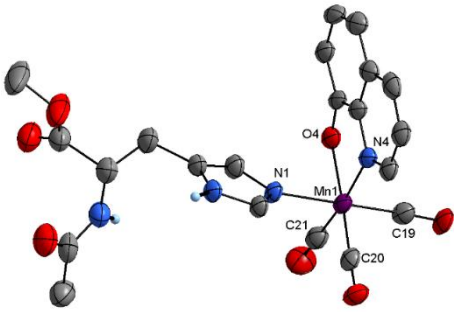

Figure 6. Crystal structure representation of **7** (CCDC 2160595). Ellipsoids are drawn with 30% probability. Solvent molecules (water and dichloromethane) and most of hydrogen atoms are omitted for the sake of clarity. Only hydrogen atoms involved in hydrogen bonds are shown. Bond lengths (Å) and angles (°) in the coordination sphere at 200 K : Mn1-O4 2.026(5), Mn1-N4 2.042(6), Mn1-C19 1.788(8), Mn1-C20 1.787(8), Mn1-C21 1.81(1), Mn1-N1 2.076(5), O4-Mn1-N4 80.6(2), O4-Mn1-C19 96.7(3), O4-Mn1-C20 174.6(2), O4-Mn1-C21 92.7(3), O4-Mn1-N1 84.62(19), N4-Mn1-C19 92.0(3), N4-Mn1-C20 95.8(3), N4-Mn1-C21 173.1(3), N4-Mn1-N1 85.7(2), C19-Mn1-C20 87.4(3), C19-Mn1-C21 90.5(4), C19-Mn1-N1 177.2(3), C20-Mn1-C21 90.8(3), C20-Mn1-N1 91.2(3), C21-Mn1-N1 91.9(3).

Spectroscopic properties. UV-visible spectra of **2-7** were recorded in acetonitrile and depicted in Fig. 7A for **2** and in Fig. S2-S6 for **3-7**. All compounds present a double-top broad absorption band between 310 and 480 nm. TD-DFT calculations produced the same absorption profile for compounds **2**-**7** in the 250-550 nm wavelength range and predict two predominant absorption bands located at ca. 315 and 415 nm (Fig. 7B). Characterization of the main transitions is achieved by considering the corresponding natural transition orbitals (NTOs) depicted in Figure 8 and Figure S8 for **2**. Interestingly, no contribution from the imidazole ligands is present in the 300-550 nm wavelength range which explains the very similar absorption spectrum of all complexes in this range. The main transitions are shown to have mostly a ligand-centered (LC) or metal-centered (MC) character between 350 and 450 nm whereas the transitions accounting for the band centered around 345 nm exhibit clear

metal-to-ligand charge transfer (MLCT) features involving both the 8-HQ ligand and the CO ligands. This observation is consistent with previous works on similar systems.[42]

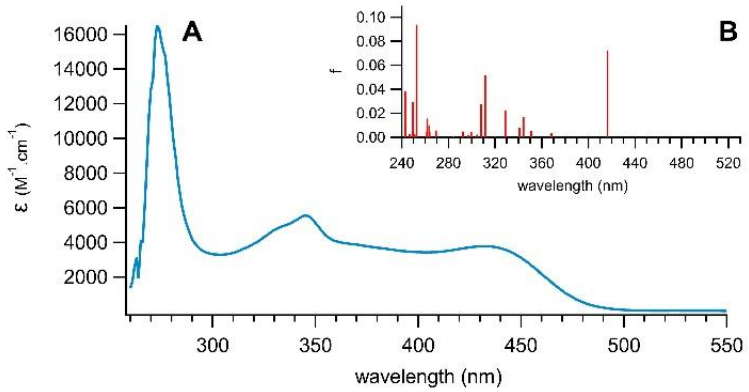

Figure 7 A. Experimental absorption spectrum of **2** recorded in acetonitrile solution and **B.** TD-DFT calculated absorption spectrum of **2** obtained at the PBE0/Def2-TZVP (PCM CAN) level of theory (f is the calculated oscillator strength).

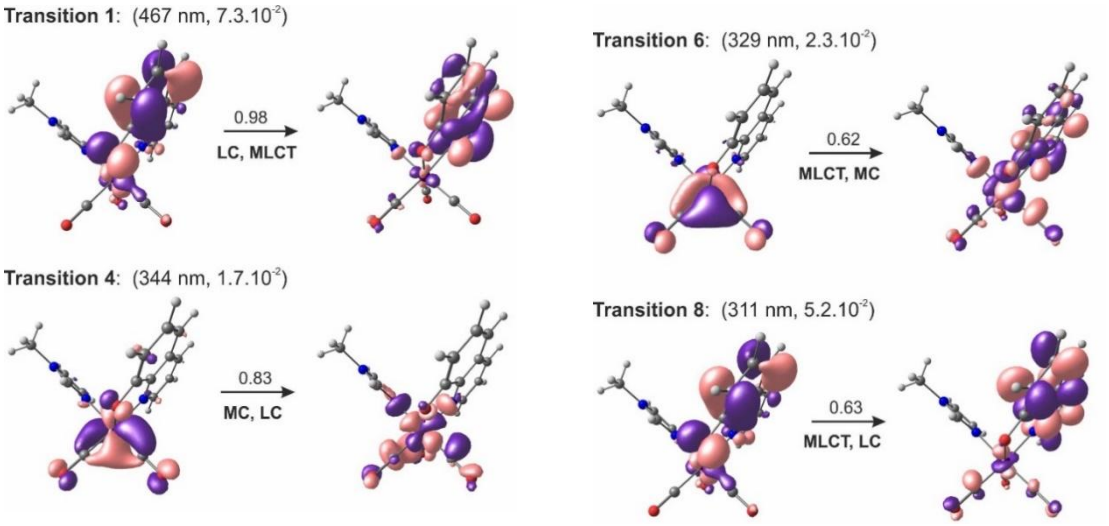

Figure 8 Natural transition orbitals for the first and main transitions of **2** in the 310-480 nm region. The excitation energy and the corresponding oscillator strengths are indicated in parentheses and the associated weights above the arrows (isodensity surface 0.043). For each transition, only the component associated to the highest weight is displayed and the main excited state character is indicated under the arrow (MLCT stands for metal-to-ligand-charge-transfer, MC for metal-centered and LC for ligand-centered charge transfer.

CO release studies. Before studying their CO releasing capacity, we first evaluated the stability of complexes **2**-**7** in acetonitrile in the dark by UV-visible spectroscopy during 18 h. As anticipated, no evolution in the UV-vis spectrum was noticed during this interval of time. When light was applied, the scenario changed dramatically. An acetonitrile solution of **2** (c = 10^{-4} M) was continuously irradiated with blue LEDs (450 nm) during 1 min, and UV-visible absorption spectra were collected

each 10 s (Figure 9). The band at 430 nm decreased in intensity over time concomitantly with a decrease in the intensity of the band at 345 nm. Simultaneously, another broad band around 380 nm appeared, suggesting the formation of a Mn^{II}(8-HQ) complex.[46] All complexes present the same behavior toward irradiation and lead to the same spectroscopic profile. A pseudo first order kinetic analysis was applied to calculate the apparent CO release rate constant and the half-life for **2**-**7** and are summarized in Table 1**.** These values echo with other manganese tricarbonyl complexes described by Braga and Peralta.[47] Interestingly, the kinetic parameters are weakly impacted by the solvent. Similar apparent kinetic constants and half-lives were obtained upon complex photolysis in acetonitrile and PBS, suggesting that the use of a strong or weak coordinating solvent did not impact the CO release. These results also underline that variation around the imidazole ring did not influence the electronic parameters and the absorption profile and the CO releasing properties seem to be guided by the 8-hydroxyquinoline ligand.

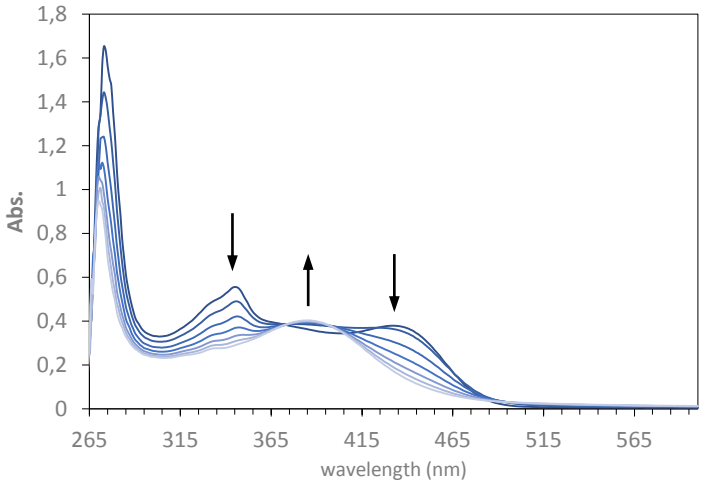

Figure 9. UV-vis spectra of **2** (c = 10^{-4} M) upon irradiation for 1 min at λ = 450 nm in acetonitrile. Spectra were collected with time interval of 10 s. The arrows indicate how the band's intensity evolves with time.

Complex	acetonitrile		PBS	
	k (s^{-1})	$t_{1/2}$ (s)	k (s^{-1})	$t_{1/2}$ (s)
2	14.7 10^{-3}	47.6	14.7 10^{-3}	47.6
3	21.5 10^{-3}	32.6	15.4 10^{-3}	45.5
4	24 10^{-3}	29.2	15.4 10^{-3}	45.5
5	20.9 10^{-3}	33.5	16.8 10^{-3}	41.7
6	20.9 10^{-3}	33.5	18.1 10^{-3}	38.7
7	17.9 10^{-3}	39.1	17.7 10^{-3}	39.5

Table 1. Apparent rate constants and half-lives of complexes **2**-**7** in acetonitrile and PBS upon their irradiation with blue light.

Next, the CO release behavior of complexes **2-7** was monitored through the standard myoglobin assay. When solutions of complexes with myoglobin and dithionite as a reducing agent were kept in the dark for 2 h, no changes were observed in the Q band region of the spectrum, indicating that carboxymyoglobin (MbCO) was absent in solution. Upon illumination, a rapid formation of MbCO was observed for all complexes as proved by the fast growth of the two bands at 540 and 577 nm in Figure 10 for **2** (see SI for other complexes). To determine the number of CO released per mole of complex, the concentration of MbCO was extracted from these curves. The curves [MbCO] = f(t) allowed the determination of the half-lives for CO release (Table 2). These results clearly indicate that 3 mol of CO were liberated per mol of complex and all complexes present a fast CO releasing profile.

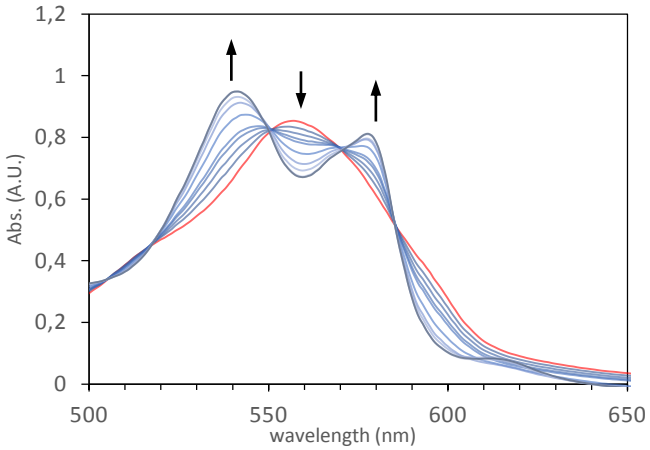

Figure 10. UV-vis absorption spectra of reduced horse skeletal myoglobin (65 µM – red line) and after addition of **2** (20 µM) in PBS (0.1 M) and continuous irradiation with blue LEDs (λ = 450 nm) for 5 min. Spectra were collected with time interval of 30 s. The arrows indicate how the band's intensity evolves with time.

Complex	Equivalents of CO	$t_{1/2}$ (s)
2	2.70	142
3	2.85	133
4	2.95	107
5	2.93	120

6	3.00	109
7	2.85	117

Table 2. Equivalents of CO released and half-lives for CO release of complexes **2**-**7**.

IR, EPR and Mass spectrometry studies. To better understand the CO release mechanism, *in-situ* infrared spectroscopy was used to monitor qualitatively the carbonyl ligands stretching vibration modes (ν_{CO}) upon simultaneous irradiation of a solution of **2** in acetonitrile at 450 nm (Figure 11). The ν_{CO} bands remained unchanged in the dark (20 min) but during light exposure, the three CO bands gradually decreased in intensity. It has been shown that manganese tricarbonyl complexes can lose a single CO resulting in the formation of a biscarbonyl species, which evolves over time by releasing its two remaining CO.[48] In our case, no change in the symmetry of the signals was observed, indicating that the formation of a biscarbonyl intermediate did not take place or that its life time was too short to be detected.

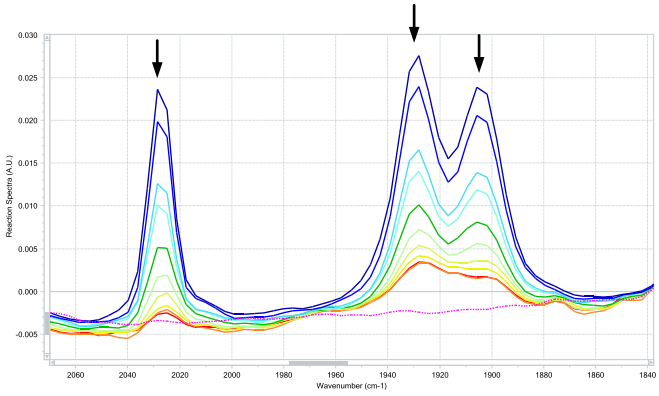

Figure 11. Evolution of the infrared spectrum of **2** during irradiation at λ = 450 nm in acetonitrile for 5 min. Spectra were collected with time interval of 30 s. The blue curve corresponds to t = 0 and the red one to t = 5 min. The arrow indicates the evolution of the band intensity with time.

The fate of the complexes after irradiation (= photoproduct) is a crucial aspect that needs to be addressed but which is also difficult to determine because the structures of inactivated CORMs (iCORMs) remain elusive in most cases. A benchmark work by Kurz on Mn-based CORMs indicates that the loss of CO occurs concomitantly with the oxidation of the metal center producing Mn^{II} and Mn^{III} species.[49] In this context, the oxidation state of complex **2** upon irradiation was investigated by X-band EPR spectroscopy. While before irradiation,

almost no signal could be detected (a negligible trace of Mn(II) could be observed), after 30 s irradiation the Mn(II) signal increases significantly (red curve, Figure 12), together with the appearance of a sharp signature at g=2, suggesting the formation of some organic radical during release of the CO ligands. This Mn(II) signal kept increasing, and after extensive photolysis (300 seconds of irradiation), only a very intense envelope (blue curve, downscaled by a factor 100, Figure 12) was observed. This reflects a broadening probably due to Mn(II) / Mn(II) through space magnetic interactions characteristic of concentrated Mn(II) solutions. Thus, these EPR experiments, consistent with some former literature reports, confirm the oxidation of the Mn(I) concomitantly to the CO release process.

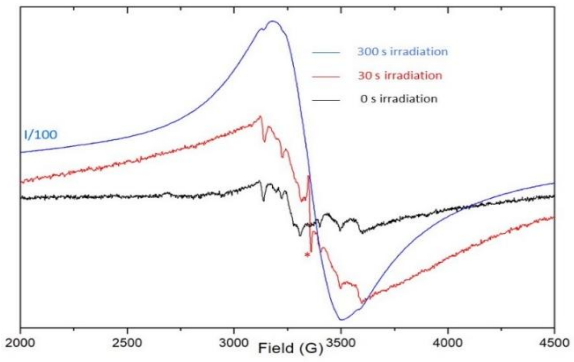

Figure 12. EPR spectra of **2** (100 µM, MeCN) recorded at various times during irradiation. *: transient organic radical detected after 30 s irradiation.

The obtained EPR spectra unambiguously indicate the formation of a Mn(II) species but without information about the spin state. Due to the high pairing energy of the electron in Mn(II),[50] low spin Mn(II) complexes are rather rare and necessitate very strong field ligands. As the CO are released, the strongest field ligand remaining in the media is 8-HQ. However, Mn(II)(8-HQ)$_2$ complex has been shown to be high-spin,[46] and thus 8-HQ is not strong enough to induce a low spin Mn(II) ion. Note that formation of a low spin Mn(II) would also induce appearance of *d-d* transition in the visible spectrum,[50] whereas the observed spectra after irradiation display typical feature of high-spin Mn(II)(8-HQ) complexes. Thus, in our case, the Mn(II) complex is very likely to be high spin. To confirm this hypothesis, the Evans method

was applied to determine the spin state of the iCORMs derived from complex **2**. A 10 mM solution of **2** in deuterated acetonitrile was extensively irradiated (60 min) to produce the corresponding iCORM, followed by NMR analysis. The chemical shift of residual acetonitrile was used for the molar magnetic susceptibility determination. According to the Evans' equation (see SI for details), the effective magnetic moment could be calculated and was found to be μ_{eff} = 5.09. The theorical values for a low-spin and high-spin Mn(II) complexes are respectively 1.73 and 5.92, confirming that the Mn(II) complex obtained after photolysis of **2** is likely to be high-spin.

Mass spectrometry experiment was conducted to investigate the structure of iCORMs derived from **2**. HRMS of a 10 µM solution of **2** in acetonitrile was recorded after extensive irradiation (60 minutes) and is depicted in Figure 13. The irradiation of the solution led to changes in the ion composition: the *m/z* 366 ion corresponding to the initial compound completely disappeared whereas two main peaks assigned to $[Mn(8\text{-}HQ)_2]^+$ and $[Mn(8\text{-}HQ)_2Me\text{-}Imd]H^+$ ions (*m/z* 343 and *m/z* 425, respectively) were obtained. This clean composition of the reaction mixture allowed us to assume that $Mn(8\text{-}HQ)_2Me\text{-}Imd$ should correspond to the iCORM of **2** and the $[Mn(8\text{-}HQ)_2]^+$ ion may derive from the Mn(II) ion after oxidation in the ionization source.

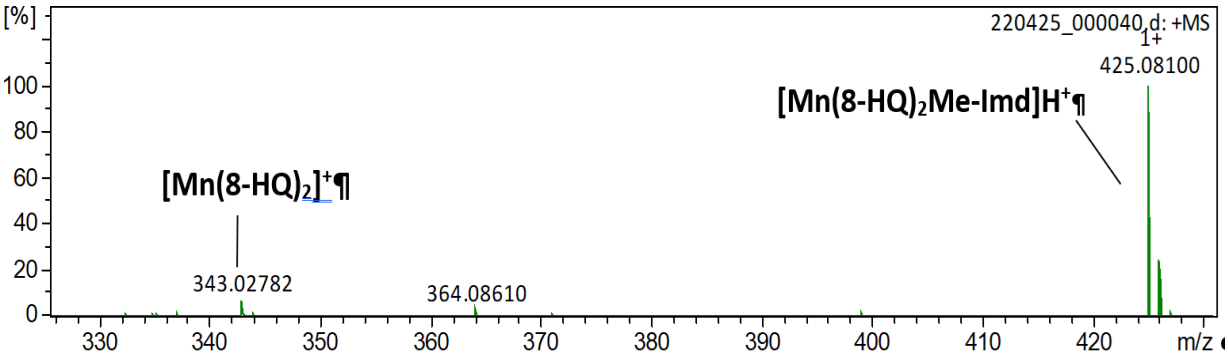

Figure 13. HRMS of **2** (10 µM, MeCN) after 60 minutes of irradiation.

Conclusions

In conclusion, we reported herein the synthesis, characterization and CO release studies of a new series of neutral Mn(I) tricarbonyl complexes having the general formula Mn(8-

HQ)$(CO)_3$(Imd)] with Imd = imidazole derivatives. All complexes were obtained by opening of the dimeric complex **1** upon treatment with imidazole derivatives in THF under mild conditions. The blue light photoinduced CO release capacities of complexes were investigated by several approaches including UV-vis, IR, TD-DFT, EPR and mass spectrometry. All the complexes present a fast CO releasing profile and enable the production of 3 moles of CO per mole of complex, along with the concomitant oxidation of the metal center leading to a new structure (iCORM) that could be formulated as Mn(8-HQ)$_2$Imd. Compounds remain stable in the dark even in a coordinating solvent such as acetonitrile and CO release only occurs after light activation. A wide range of imidazole ligands was successfully applied, including a more advanced ligand derived from histidine. The direct utilization of imidazole and by extension histidine as a ligand could open new perspectives for the late-stage functionalization of peptides or proteins with CORMs notably through the functionalization of poly-histidine tails as a strategy to conjugate biologically meaningful vectors for site-selective delivery of photoCORMs.

Author Contributions

Marcel Annereau: data curation, investigation, writing – review and editing. **Franck Martial:** investigation, writing – review and editing. **Jérémy Forté:** data curation, formal analysis, investigation, writing – original draft preparation, writing – review and editing. **Geoffrey Gontard:** data curation, formal analysis, investigation, writing – original draft preparation, writing – review and editing. **Sébastien Blanchard:** data curation, investigation, writing – original draft preparation, writing – review and editing. **Héloïse Dossmann:** data curation, formal analysis, investigation, writing – original draft preparation, writing – review and editing. **Michèle Salmain:** supervision, writing – original draft preparation, writing – review and editing. **Vincent Corcé:** conceptualization, data curation, formal analysis, investigation, project administration, supervision, validation, writing – original draft preparation, writing – review and editing.

Acknowledgements

We thank Sorbonne Université and CNRS for financial support. This work was granted access to the HPC resources of the HPCaVe centre at Sorbonne Université. Financial support from the IR FT-ICR FR3624 for conducting the research is also gratefully acknowledged. Claire Troufflard and Régina Maruchenko are warmly acknowledged for NMR assistance.

References

[1] B. Widdop, *Ann. Clin. Biochem.* **2002**, *39*, 378–391.
[2] C. G. Douglas, J. S. Haldane, J. B. S. Haldane, *J. Physiol.* **1912**, *44*, 275–304.
[3] S. H. Heinemann, T. Hoshi, M. Westerhausen, A. Schiller, *Chem. Commun.* **2014**, *50*, 3644–3660.
[4] J. M. Fukuto, S. J. Carrington, D. J. Tantillo, J. G. Harrison, L. J. Ignarro, B. A. Freeman, A. Chen, D. A. Wink, *Chem. Res. Toxicol.* **2012**, *25*, 769–793.
[5] B. A. Moore, M. Overhaus, J. Whitcomb, E. Ifedigbo, A. M. K. Choi, L. E. Otterbein, A. J. Bauer, *Crit. Care Med.* **2005**, *33*, 1317–1326.
[6] S. W. Ryter, J. Alam, A. M. K. Choi, *Physiol. Rev.* **2006**, *86*, 583–650.
[7] L. E. Otterbein, F. H. Bach, J. Alam, M. Soares, H. Tao Lu, M. Wysk, R. J. Davis, R. A. Flavell, A. M. K. Choi, *Nat. Med.* **2000**, *6*, 422–428.
[8] R. Motterlini, L. E. Otterbein, *Nat. Rev. Drug Discov.* **2010**, *9*, 728–743.
[9] C. C. Romão, W. A. Blättler, J. D. Seixas, G. J. L. Bernardes, *Chem. Soc. Rev.* **2012**, *41*, 3571–3583.
[10] K. Ling, F. Men, W.-C. Wang, Y.-Q. Zhou, H.-W. Zhang, D.-W. Ye, *J. Med. Chem.* **2018**, *61*, 2611–2635.
[11] A. C. Kautz, P. C. Kunz, C. Janiak, *Dalton Trans.* **2016**, *45*, 18045–18063.
[12] L. K. Wareham, R. K. Poole, M. Tinajero-Trejo, *J. Biol. Chem.* **2015**, *290*, 18999–19007.
[13] J. Cheng, J. Hu, *ChemMedChem* **2021**, *16*, 3628–3634.
[14] N. Abeyrathna, K. Washington, C. Bashur, Y. Liao, *Org. Biomol. Chem.* **2017**, *15*, 8692–8699.
[15] S. García- Gallego, G. J. L. Bernardes, *Angew. Chem. Int. Ed.* **2014**, *53*, 9712–9721.
[16] X. Jiang, Z. Xiao, W. Zhong, X. Liu, *Coord. Chem. Rev.* **2021**, *429*, 213634.
[17] J. Marhenke, K. Trevino, C. Works, *Coord. Chem. Rev.* **2016**, *306*, 533–543.
[18] R. Weinstain, T. Slanina, D. Kand, P. Klán, *Chem. Rev.* **2020**, *120*, 13135–13272.
[19] S. Romanski, B. Kraus, U. Schatzschneider, J.-M. Neudörfl, S. Amslinger, H.-G. Schmalz, *Angew. Chem. Int. Ed.* **2011**, *50*, 2392–2396.
[20] S. Romanski, E. Stamellou, J. T. Jaraba, D. Storz, B. K. Krämer, M. Hafner, S. Amslinger, H. G. Schmalz, B. A. Yard, *Free Radic. Biol. Med.* **2013**, *65*, 78–88.
[21] P. C. Kunz, H. Meyer, J. Barthel, S. Sollazzo, A. M. Schmidt, C. Janiak, *Chem. Commun.* **2013**, *49*, 4896–4898.

[22] B. J. Aucott, J. S. Ward, S. G. Andrew, J. Milani, A. C. Whitwood, J. M. Lynam, A. Parkin, I. J. S. Fairlamb, *Inorg. Chem.* **2017**, *56*, 5431–5440.
[23] X. Ji, L. K. C. D. L. Cruz, Z. Pan, V. Chittavong, B. Wang, *Chem. Commun.* **2017**, *53*, 9628–9631.
[24] T. Storr, K. H. Thompson, C. Orvig, *Chem. Soc. Rev.* **2006**, *35*, 534–544.
[25] R. G. Kenny, C. J. Marmion, *Chem. Rev.* **2019**, *119*, 1058–1137.
[26] W. O. Foye, J. R. Marshall, *J. Pharm. Sci.* **1964**, *53*, 1338–1341.
[27] Gaussian, Inc., Wallingford CT, 2019, **n.d.**
[28] F. Weigend, R. Ahlrichs, *Phys. Chem. Chem. Phys.* **2005**, *7*, 3297–3305.
[29] C. Adamo, V. Barone, *J. Chem. Phys.* **1999**, *110*, 6158–6170.
[30] J. P. Perdew, M. Ernzerhof, K. Burke, *J. Chem. Phys.* **1996**, *105*, 9982–9985.
[31] J. Tomasi, B. Mennucci, R. Cammi, *Chem. Rev.* **2005**, *105*, 2999–3094.
[32] R. L. Martin, *J. Chem. Phys.* **2003**, *118*, 4775–4777.
[33] https://www.chemcraftprog.com, **n.d.**
[34] A. J. Atkin, J. M. Lynam, B. E. Moulton, P. Sawle, R. Motterlini, N. M. Boyle, M. T. Pryce, I. J. S. Fairlamb, *Dalton Trans.* **2011**, *40*, 5755–5761.
[35] C. Bischof, T. Joshi, A. Dimri, L. Spiccia, U. Schatzschneider, *Inorg. Chem.* **2013**, *52*, 9297–9308.
[36] M. Albrecht, M. Fiege, O. Osetska, *Coord. Chem. Rev.* **2008**, *252*, 812–824.
[37] D. A. Habashy, R. M. Khaled, A. Y. Ahmed, K. Radacki, S. K. Ahmed, E. K. Tharwat, H. Magdy, A. Zeinhom, A. M. Mansour, *Dalton Trans.* **2022**, *51*, 14041–14048.
[38] P. J. Parker, A. Wojcicki, *Inorganica Chim. Acta* **1974**, *11*, 17–23.
[39] P. J. Parker, A. Wojcicki, *Inorganica Chim. Acta* **1974**, *11*, 9–16.
[40] M. McKinnon, K. T. Ngo, S. Sobottka, B. Sarkar, M. Z. Ertem, D. C. Grills, J. Rochford, *Organometallics* **2019**, *38*, 1317–1329.
[41] H. C. Zhao, B. Mello, B.-L. Fu, H. Chowdhury, D. J. Szalda, M.-K. Tsai, D. C. Grills, J. Rochford, *Organometallics* **2013**, *32*, 1832–1841.
[42] T.-W. Tseng, S. Mendiratta, T.-T. Luo, T.-W. Chen, Y.-P. Lee, *Inorganica Chim. Acta* **2018**, *477*, 312–317.
[43] P. V. Simpson, C. Nagel, H. Bruhn, U. Schatzschneider, *Organometallics* **2015**, *34*, 3809–3815.
[44] R. A. Sykes, P. McCabe, F. H. Allen, G. M. Battle, I. J. Bruno, P. A. Wood, *J. Appl. Crystallogr.* **2011**, *44*, 882–886.
[45] I. Dance, *New J. Chem.* **2003**, *27*, 22–27.
[46] L. M. A. Monzon, F. Burke, J. M. D. Coey, *J. Phys. Chem. C* **2011**, *115*, 9182–9192.
[47] A. L. Amorim, M. M. Peterle, A. Guerreiro, D. F. Coimbra, R. S. Heying, G. F. Caramori, A. L. Braga, A. J. Bortoluzzi, A. Neves, G. J. L. Bernardes, R. A. Peralta, *Dalton Trans.* **2019**, *48*, 5574–5584.
[48] V. C. Weiss, G. Farias, A. L. Amorim, F. R. Xavier, T. P. Camargo, M. B. Bregalda, M. Haukka, E. Nordlander, B. de Souza, R. A. Peralta, *Inorg. Chem.* **2020**, *59*, 13078–13090.
[49] H.-M. Berends, P. Kurz, *Inorganica Chim. Acta* **2012**, *380*, 141–147.
[50] A. B. P. Lever, *Inorganic Electronic Spectroscopy*, Elsevier, New York, **1984**.